Journal of Cranio-Maxillo-Facial Surgery 47 (2019) 245–254

Contents lists available at ScienceDirect

Journal of Cranio-Maxillo-Facial Surgery

journal homepage: www.jcmfs.com

Three-dimensional analyses of nasolabial forms and upper lip surface symmetry after primary lip repair in patients with complete unilateral cleft lip and palate

Namiko Kimura, Etsuro Nozoe, Takako Okawachi, Kiyohide Ishihata, Takao Fuchigami, Norifumi Nakamura*

Department of Oral and Maxillofacial Surgery, Field of Oral and Maxillofacial Rehabilitation, Kagoshima University Graduate School of Medical and Dental Sciences, 8-35-1 Sakuragaoka, Kagoshima, 890-8544, Japan

ARTICLE INFO

Article history:
Paper received 22 September 2018
Accepted 29 November 2018
Available online 5 December 2018

Keywords:
Cleft lip and palate
Lip and nose forms
Three-dimensional morphology
Vectra H1
Histogram intersection

ABSTRACT

Purpose: To analyze three-dimensional (3D) nasolabial forms and upper lip surface symmetry after primary lip repair in children with unilateral cleft lip and palate (UCLP).
Methods: Subjects were 22 Japanese children with complete UCLP who underwent primary lip repair and were followed-up for 4–6 years. The 3D coordinates of facial landmarks and the angle and radius of the approximate nasal alar circle were calculated. Upper lip surface symmetry was analyzed using histogram intersection.
Results: The nasal tip and columella base were slightly dislocated to the cleft side, and the midpoint of Cupid's bow shifted to the non-cleft side. The nasal alar and the top of Cupid's bow were reconstructed at the same height, while the approximate nasal alar circle was smaller on the cleft side. The mean value of similarity for upper lip surface symmetry was 0.82; a subject with a higher value had more symmetrical contour lines in the visualized surface image.
Conclusions: Postoperative nasolabial forms were almost restored to symmetrical levels, while retaining a small nasal alar. Histogram intersection is applicable as a method for the quantitative evaluation of upper lip surface symmetry in UCLP.

1. Introduction

The ultimate goal of primary lip repair for patients with unilateral cleft lip and palate (UCLP) is to reconstruct symmetrical and natural forms of the lip and nose, and to achieve a smooth upper lip surface without any conspicuous scars (Nkenke et al., 2006; Chou et al., 2013; Matsunaga et al., 2016; Mosmuller et al., 2016). Various cleft surgeries using a range of skin incision techniques have been reported to date (Cronin, 1966; Millard, 1976; Fisher, 2005). Despite recent developments in cleft surgery, postoperative asymmetrical and deformed nasolabial forms in patients with complete UCLP remain a problem (Bugaighis et al., 2010; Okawachi et al., 2011). In order to reach the goal of cleft lip surgery, it is essential to consider cleft-related deformity as an important component of the quality of life outcome for patients with UCLP, so precise measures need to be taken in order to comprehensively assess the effects of treatments for CLP (Al-Omari et al., 2005). These results can then be used as feedback to guide improvements to surgical procedures for subsequent cleft lip repair.

Regarding methods of assessing the nasolabial forms of patients with unilateral and bilateral cleft lip, many direct clinical measurements (Al-Omari et al., 2005), as well as two-dimensional (2D) (Al-Omari et al., 2005; Nakamura et al., 2009; Berssenbrügge et al., 2014; Matsunaga et al., 2016) and three-dimensional (3D) evaluations (Nkenke et al., 2006; Bugaighis et al., 2010; He et al., 2010; Nakamura et al., 2010; Okawachi et al., 2011; Li et al., 2013; Tse et al., 2014; Wu et al., 2016; Liang et al., 2017) have been reported to date. Until a decade ago, digital 2D photographs were commonly examined in morphological analyses (Bugaighis et al., 2010).

* Corresponding author. Department of Oral and Maxillofacial Surgery, Field of Oral and Maxillofacial Rehabilitation, Kagoshima University Graduate School of Medical and Dental Sciences, 8-35-1 Sakuragaoka, Kagoshima, 890-8544, Japan. Fax: +81 99 275 6248.
E-mail address: nakamura@dent.kagoshima-u.ac.jp (N. Nakamura).

https://doi.org/10.1016/j.jcms.2018.11.035
1010-5182/

However, 2D assessments are limited because of the lack of information on facial depth and shape (Da Silveira et al., 2003; Knoops et al., 2017). Li et al. (2013) reported that 2D photography data were influenced by many factors, including the distance and angle from which the photograph was taken, so linear and angular measurements using 2D photographs can vary markedly. Since nasolabial deformations on patients with CLP are three-dimensional (Campbell et al., 2010), 3D morphological assessments are needed in order to evaluate the outcomes of CLP treatments.

More 3D analyses of the facial morphologies of patients with CLP have been performed in recent years with the development of 3D measuring technology and devices (Nkenke et al., 2006; Bugaighis et al., 2010; He et al., 2010; Nakamura et al., 2010; Li et al., 2013; Tse et al., 2014; Wu et al., 2016; Knoops et al., 2017; Liang et al., 2017). We have performed 3D analyses of the lip and nose forms of unilateral and bilateral CLP patients who underwent secondary CLP treatment, using a non-contact laser scanner (Nakamura et al., 2011; Okawachi et al., 2011). However, for the assessment of postoperative facial forms of infants or young children with UCLP, who had undergone primary lip and nose repair, we analyzed postoperative lip and nose forms using 2D photography (Nakamura et al., 2009; Matsunaga et al., 2016). This was because it was difficult for the young patients to remain still enough for scanning of facial forms using a laser scanner.

Advances have been made in image acquisition methods based on the principle of stereophotogrammetry. With this system, the image capturing time is very short and, thus, it is useful for taking images of infants and young children (Al-Omari et al., 2005; He et al., 2010; Nakamura et al., 2010; Tse et al., 2014; Liang et al., 2017). In our department, we have adopted the non-invasive Vectra H1® 3D image scanning device (Canfield Scientific, Inc. America), which is a compact and simple handheld device that is able to rapidly capture facial images in clinical settings. It is thus suitable for the 3D evaluation of postoperative nasolabial forms in infants and young children following primary lip repair.

For assessment of the position and the symmetry of nasolabial forms in patients with CLP, 3D analysis, in which some landmarks were set, and the positions and linear and angular measurements were taken using the 3D coordinates of these landmarks, have been reported (Yamada et al., 2002; Nkenke et al., 2006; Stauber et al., 2008). However, with evaluation measurements using points, it is impossible to reflect a complicated 3D form, and evaluation of symmetry becomes more localized (Meyer-Marcotty et al., 2010), so that accurate and global measurements of skin surface forms on the upper lip may be difficult to achieve.

In this study, in order to analyze 3D nasolabial forms following primary lip and nose repair in young children with complete UCLP, 3D facial images were captured using the Vectra H1®. Facial landmarks were measured three-dimensionally and similarities analyzed in order to assess the symmetry of upper lip skin surface forms, using histogram intersection as new quantitative assessment method.

2. Materials and methods

2.1. Patients

Subjects in this study included 22 patients, 10 boys and 12 girls, with complete UCLP, who underwent primary lip repair in accordance with our treatment procedure (Nakamura et al., 2009; Fuchigami et al., 2014; Matsunaga et al., 2016) between 2009 and 2013. Procedures were carried out by the same surgeon in the Department of Oral and Maxillofacial Surgery, Kagoshima University Medical and Dental Hospital. The treatment schedule included the following: 1) presurgical orthopedics using NAM from birth to primary lip repair, in order to minimize surgical intervention; 2) primary lip repair by the modified Cronin's triangular-flap method (Cronin, 1966) at 3–6 months old (mean age 5.1 ± 1.6 months); 3) simultaneous medial-upward advancement of nasolabial components, which allows repositioning of the lower lateral cartilage on the affected side; 4) vestibular expansion using a cleft margin flap to provide the vertical height of the nasal alar and nostrils, and to minimize deformations due to postoperative regression; and 5) reconstruction of the orbicularis oris muscle, pars peripheralis, and pars marginalis, with overlapping, inter-digitation, and edge-to-edge suturing, in order to reconstruct forms corresponding with the philtrum column (Nakamura et al., 2009; Fuchigami et al., 2014; Matsunaga et al., 2016).

Data were collected from the records of the CLP Team at Kagoshima University Medical and Dental Hospital. This study was approved by the Kagoshima University Medical and Dental Hospital Institutional Review Board, and all participants provided informed consent.

2.2. Scanning device, image processing software, and data capture technique

The 3D facial images of patients were captured using the non-invasive Vectra H1® 3D image scanner. The age at photographing was 4–6 years (mean 5.3 years ±11.5 months). The patient's face was captured from the front and diagonally downwards at an angle of 45° on the right and left sides using the Vectra H1®. Each patient's facial image was captured several times, and images with similar expressions were selected and used. In order not to induce differences in expression, the patients were in a calm environment and images were taken when the face was at rest. These facial images were then imported into the software Mirror Photo Tool® (Canfield Scientific, Inc., America) and selected and stitched to generate one 3D facial image (Camison et al., 2018).

2.3. Setting the reference plane

In the next step — setting the reference plane — measurements and analyses of nasolabial forms were performed using the 3D image software 3D-Rugle 7® (Medic Engineering, Inc., Kyoto, Japan). 3D-reconstructed facial images were compiled and standardized to face in the same direction, such that all clefts were presented on the left side. In each 3D facial image, the midpoint between the left and right endocanthion points (En) was set as the origin (point O: $x = 0, y = 0$, and $z = 0$). The straight line passing through the left and right En was set as the x-axis, and the reference plane passing through three points — the right and left En and nasal alar base point (Alb) on the non-cleft side — was set as the x–y plane. The straight line passing through the origin point and perpendicularly crossing the x-axis was set as the y-axis. Finally, the straight line passing through the origin point and crossing the x–y plane perpendicularly was set as the z-axis (Fig. 1A). The reference plane was assessed five separate times for each 3D-reconstructed facial image. All procedures, including capturing, constructing, and analyzing 3D images, were performed by one examiner (NK) in order to avoid inter-examiner errors.

2.4. Facial landmarks

In order to assess nasolabial forms, 17 facial landmarks were detected on 3D facial images and placed manually onto texture images, while displaying normal vector images, in order to define facial structures more clearly (Table 1 and Fig. 1A and B). Among these, 1–15 landmarks were found to match the anatomical locations used in previous studies of the nasolabial forms for patients with CLP (Yamada et al., 2002; Bilwatsch et al., 2006; Nkenke et al., 2006; Stauber et al., 2008). Another two points, Alb on the non-cleft and cleft sides (points 16 and 17, respectively), were identified as

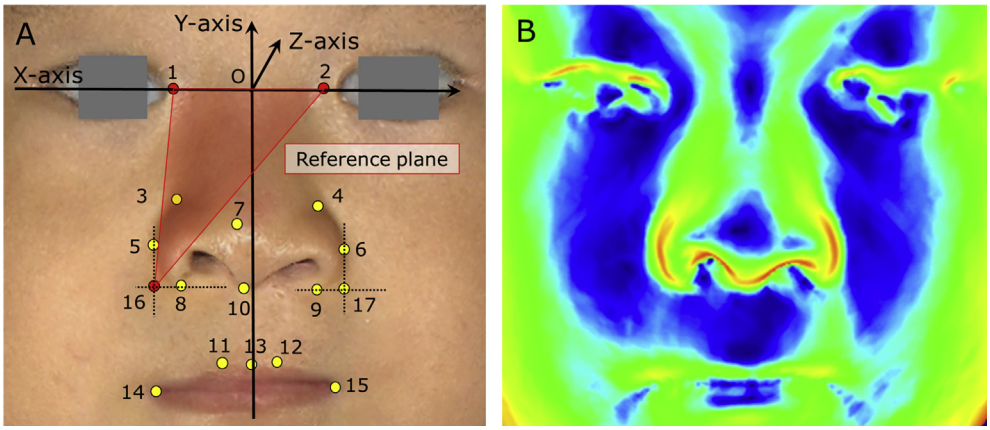

Fig. 1. (A) The reference plane, axis, and facial landmarks 1–17 on a 3D facial texture image (front view). In order to determine the reference plane, the midpoint between the right and left endocanthion points was established as the origin ($x = 0$, $y = 0$, and $z = 0$). The plane containing the origin, left or right endocanthion, and the nasal alar base point of the non-cleft side was defined as the x–y plane ($z = 0$). (B) A normal vector image. Between 1 and 15 anatomical facial landmarks were placed while referring to this vector image.

Table 1
Facial landmarks.

No.	Abbreviation	Facial landmarks
1, 2	En	Endocanthion points of the non-cleft and cleft sides
3, 4	G. sup	Most superior points of the alar groove of the non-cleft and cleft sides
5, 6	G. lat	Most lateral points of the alar groove of the non-cleft and cleft sides
7	Prn	Pronasale, nasal tip point; the highest point on the nasal tip
8, 9	G. base	Most inferior points of the alar groove of the non-cleft and cleft sides
10	Col	Columellar base point; subnasal point
11, 12	Lt	Top points of Cupid's bow of the non-cleft and cleft sides
13	Lm	Midpoint of Cupid's bow
14, 15	Ch	Cheilion points of the non-cleft and cleft sides; the point located at each labial commissure
16, 17	Alb	Alar base points of the non-cleft and cleft sides; the intersection point of the straight line passing through the most lateral point on the alar groove of the non-cleft and cleft sides and the straight line passing through the Col point. The x-coordinate of point 16 (17) is the same as the x-coordinate of point 5 (6), and the y-coordinate of point 16 (17) is the same as the y-coordinate of point 8 (9).

the intersection point of the straight line passing through the most lateral point of the alar groove (G. lat) on the non-cleft and cleft sides and the straight line passing through the most inferior point on the alar groove (G. base) on the non-cleft and cleft sides. On each subject, the 3D coordinates of 17 facial landmarks were measured five times and the mean value of each 3D coordinate was used in the four measurement items discussed below.

2.5. Measurement items

2.5.1. Reliability of reference plane and facial landmarks

Prior to this study, we assessed the reproducibility of the reference plane and facial landmarks by measuring each landmark five times. The reliability ($\sum\alpha$) — the standard deviation of the average value (standard error) — was calculated using the following formula:

$$\sum \alpha = \sqrt{\frac{\sum \Delta^2}{n(n-1)}}$$

The residual error (Δ) is the difference between the average value of five measurements and each measured value.

2.5.2. 3D measurements of facial landmarks

In the assessment of the midline of the face, the x-coordinates of the nasal tip (Prn; point 7), columella base point (Col; point 10), and midpoint of Cupid's bow (Lm; point 13) were calculated (Fig. 2A).

In evaluating the difference in the cephalocaudal height of the lip and nose between the cleft and non-cleft sides, the distance from the x-axis to the superior point of the alar groove (G. sup) on the non-cleft and cleft sides (points 3 and 4), to G. lat on the non-cleft and cleft sides (points 5 and 6), to G. base on the alar groove of the non-cleft and cleft sides (points 8 and 9), and to the top of Cupid's bow (Lt) on the non-cleft and cleft sides (points 11 and 12) were measured (Fig. 2B).

In addition, for the comparison of the anteroposterior gap of the lip and nose between the cleft and non-cleft sides, the z-coordinates of the above eight points (3, 4, 5, 6, 8, 9, 11, and 12) were calculated.

2.5.3. Assessment of the symmetry of nasal alar forms

In order to assess the symmetry of the nasal alar forms, the nasal angle and the radius of the approximate circle of the nasal alar were calculated with reference to the measuring method reported by Okawachi et al. (2011). The nasal alar angle on the non-cleft side ($\angle$7–5–10) and that on the cleft side ($\angle$7–6–10) were calculated (Fig. 2C). Furthermore, the radius of the approximate circle of the nasal alar that was indicated by the five points on the nasal alar groove was calculated on the non-cleft side (R) and on the cleft side (r) (Fig. 2D). After the approximate circle was projected on the x–y plane, each radius of curvature was calculated using Rugle 7® software. The ratio of the curvature radius (r/R) was then calculated in order to evaluate the symmetry of the nasal form.

2.5.4. The symmetry of the upper lip surface using the histogram intersection

In the assessment of the upper lip surface, the measurement area was defined as that surrounded by points 10–17, as shown in

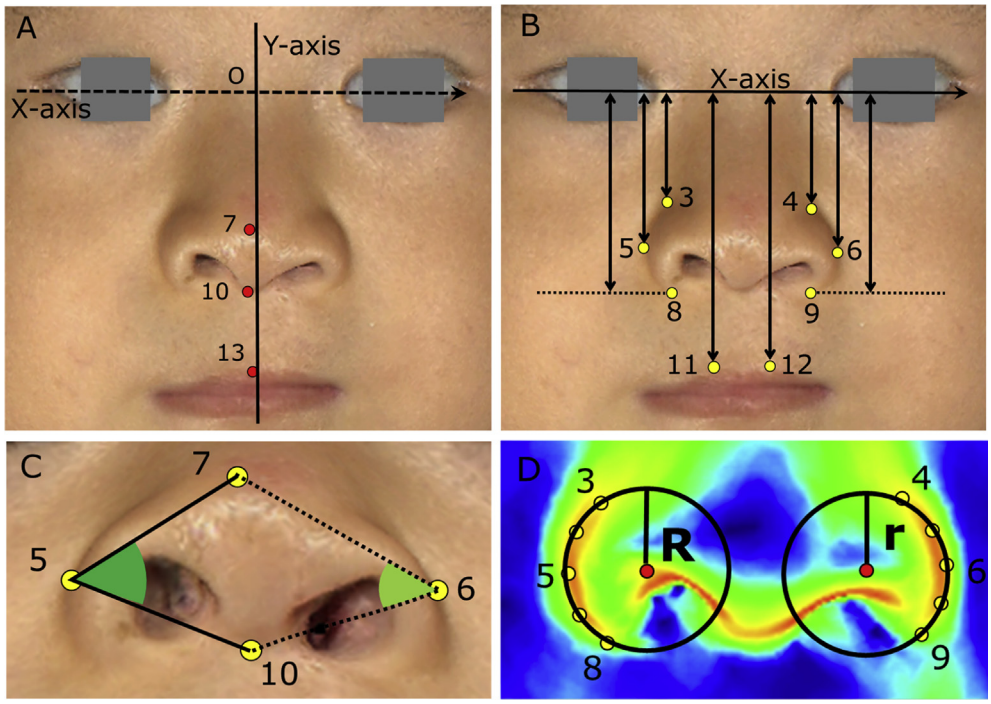

Fig. 2. Demonstration of 3D measurements using facial landmarks. (A) The nasal tip (Prn; point 7), the columellar base point (Col; point 10), and the midpoint of Cupid's bow (Lm; point 13) with the midline (the *y*-axis). (B) The distance from the *x*-axis to each point: to the superior point of the alar groove (G. sup) of the non-cleft and cleft sides (points 3 and 4); to the lateral point of the alar groove (G. lat) of the non-cleft and cleft sides (points 5 and 6); to the inferior point of the ala groove (G. base) of the non-cleft and cleft sides (points 8 and 9); and to the top point of Cupid's bow (Lt) of the non-cleft and cleft sides (points 11 and 12). (C) The nasal alar angle on the non-cleft side (∠7-5-10) and that on the cleft side (∠7-6-10). (D) The radius of the approximate circle of the nasal alar groove on the non-cleft side (R) and that on the cleft side (r).

Fig. 3A. 3D images of this area were cropped on a PC, and some of the vermilion was removed. The upper lip measurement area was then converted into a contoured, color-coded display using an anteroposterior height interval of 1.0 mm (Fig. 3B left). This area was then divided using the line connecting Col (point 10) and Lm (point 13) (Fig. 3B right). The numbers of pixels of each color on the divided upper lip areas on the cleft and non-cleft sides were counted, and the similarity of the two areas was calculated using the histogram intersection.

The histogram intersection is an algorithm that was proposed by Swain et al. (1991) as a method for judging similarities between two images (Swain and Ballard, 1991). It compares the distribution of pixels, such as particular colors included in the image, for each histogram class and thus determines the similarity between the two images. Fig. 4 shows the process for assessing symmetry of the upper lip surface using histogram intersection. The right side area of the upper lip on the non-cleft side was defined as image R, and the left-side area on the cleft side was defined as the image L. After the total numbers of pixels for each of the two images were adjusted to the same number of pixels, the pixel number for each color - pink, red, orange, yellow, yellow green, green, pale blue, blue, and dark blue - were calculated and displayed as histograms R and L. The value of similarity between image R and image L, $H(\mathrm{R},\mathrm{L})$, was defined by the following formula:

$$H(\mathrm{R},\mathrm{L}) = \frac{\sum_{j=1}^{n}\min(\mathrm{R_j},\mathrm{L_j})}{\sum_{j=1}^{n}\mathrm{R_j}}$$

In this formula, the denominator was the sum of the pixels on histogram R, and the numerator was the sum of the number of smaller pixels of each color class between histogram R and histogram L. The match value (H) varied from 0.0 to 1.0 and the closer the match value was to 1.0, the more similar the two images appeared to be (Fig. 4).

2.6. Statistical analyses

The Student's *t*-test was used to compare the mean values of all measurements of nasolabial forms between the cleft and non-cleft sides. Differences were considered to be significant when the *p*-value was less than 0.05.

3. Results

3.1. Reliability of the reference plane and facial landmarks

The reliabilities of all facial landmarks were shown in box-and-whisker plots (Fig. 5A–C). The mean reliability of En on the non-cleft side (point 1) was 0.150 mm for the *x*-coordinate, 0.076 mm for the *y*-coordinate, and 0.056 mm for the *z*-coordinate. The mean reliability of En on the cleft side (point 2) was 0.128 mm for the *x*-coordinate, 0.058 mm for the *y*-coordinate, and 0.064 mm for the *z*-coordinate. The mean reliability of Alb on the non-cleft side (point 16) was 0.177 mm for the *x*-coordinate, 0.170 mm for the *y*-coordinate, and 0.155 mm for in the *z*-coordinate. Regarding the reliabilities of the three points constituting the reference plane, 75% of the measured values for the *x*-, *y*-, and *z*-coordinates were within 0.2 mm.

Of the 3D coordinates for other facial landmarks, cheilion points (Ch) on the non-cleft side (point 14) had the largest reliability value of greater than 0.8 mm, whereas 75% of the measured values for the *x*-coordinate for all other points were within 0.5 mm (Fig. 5A). There were no landmarks with reliability greater than 0.5 mm for the *y*-coordinate, except for G. lat (point 5) on the cleft side, for

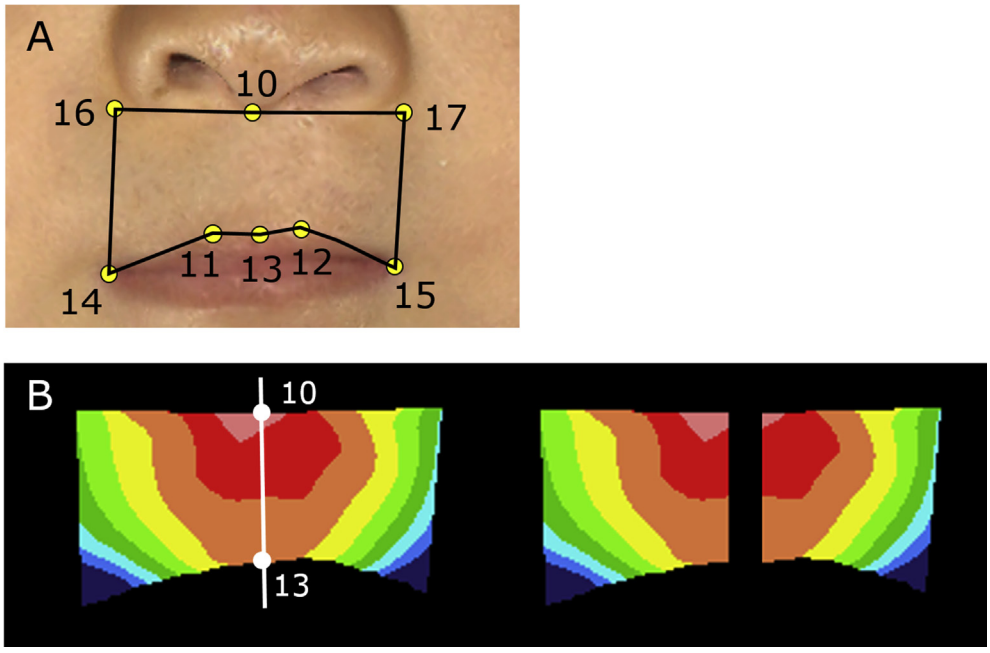

Fig. 3. Demonstration of the 3D assessment of the upper lip surface symmetry. (A) The upper lip region cropped by points 10–17 from the 3D facial image. (B) The upper lip region converted into a color-coded display, contoured at an anteroposterior height interval of 1.0 mm. The upper lip image was divided by the line connecting Col (point 10) and Lm (point 13). In order to evaluate the symmetry of the upper lip surface, the number of pixels of each color on two regions were counted and the similarity between the two areas was calculated using histogram intersection.

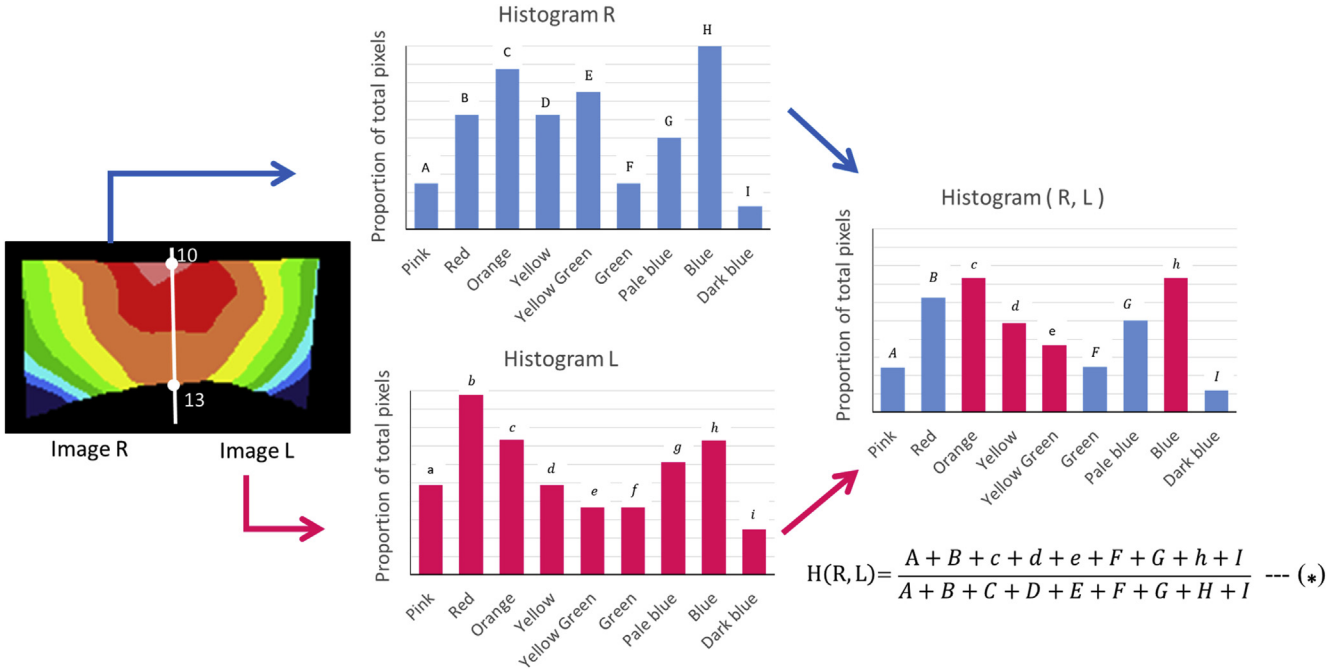

Fig. 4. In the upper lip image, which was divided by the line connecting Col (point 10) and Lm (point 13), the right side area of the upper lip (the non-cleft side) was defined as image R, and the left one (the cleft side) was defined as the image L. Histogram shows the pixels of each color class for images R and L. The number of pixels of image L were adjusted to the same number of pixels of image R. The pixels of each color - pink, red, orange, yellow, yellow green, green, pale blue, blue and dark blue - was calculated and displayed as histogram (R, L). A, B, C, D, E, F, G, H, and I were the pixels of the colors- pink, red, orange, yellow, yellow green, green, pale blue, blue and dark blue- in image R. a, b, c, d, e, f, g, h, and i were the pixels of the same colors in image L. The match value between two images could be obtained from the histogram using the formula described in the text. The denominator was the sum of the pixels on histogram R, and the numerator was the sum of the number of smaller pixels of each color class between histogram R and histogram L. In this figure, the smaller values of two histograms; A + B + c + d + e + F + G + h + I were included in the numerator.

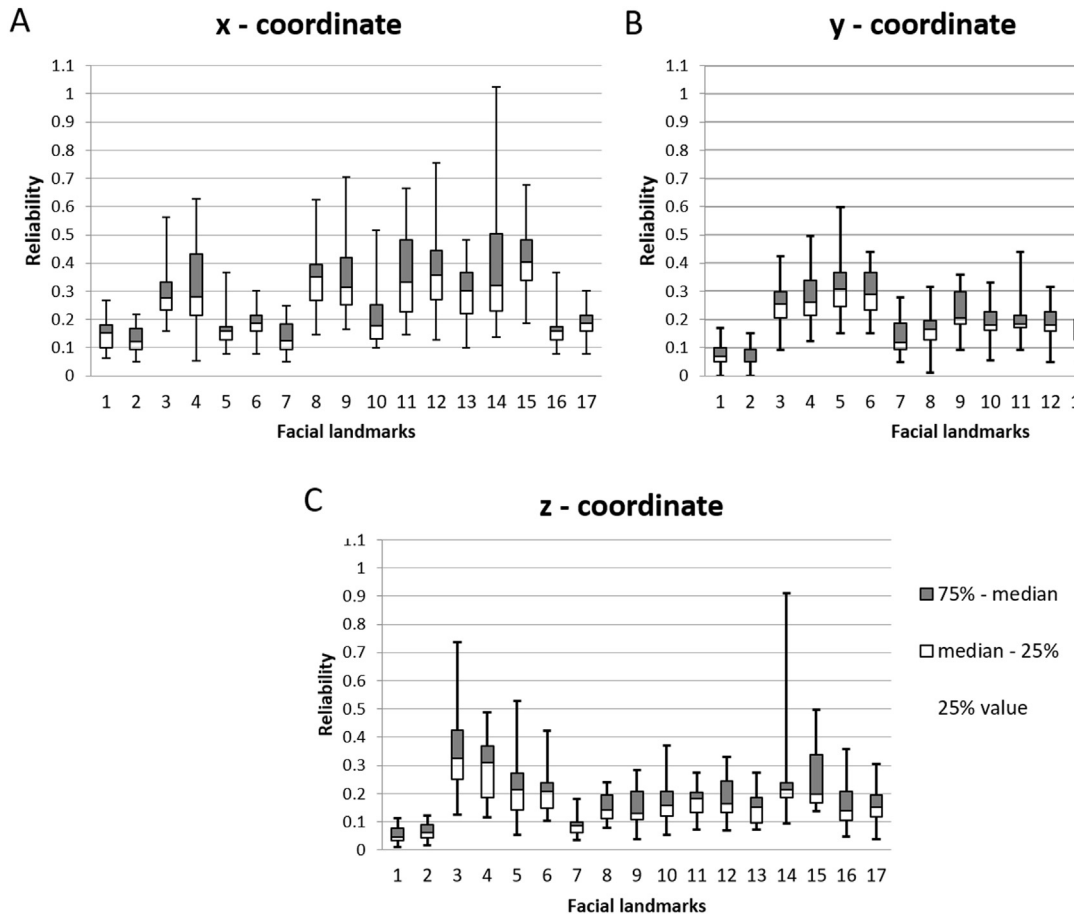

Fig. 5. The reliabilities of all measuring points, displayed as box-and-whisker plots, for (A) the *x*-coordinate, (B) the *y*-coordinate, and the *z*-coordinate.

which the maximal value was 0.6 mm (Fig. 5B). For the *z*-coordinate, Ch on the non-cleft side (point 14), reliability was greater than 0.8 mm, whereas 75% of measured values were within 0.5 mm (Fig. 5C).

3.2. 3D measurement of facial landmarks

The mean and SD for the *x*- and *y*-coordinates of each facial landmark are shown in Fig. 6. Regarding the three points relating to the midline of the face, the *x*-coordinate value was −0.87 ± 0.30 mm for Prn (point 7), −0.71 ± 1.03 for Col (point 10), and 1.17 ± 1.10 for Lm (point 13). Prn and Col dislocated to the cleft side, while Lm shifted to the non-cleft side.

The cephalocaudal distances from the *x*-axis to the nasal alar and upper lip points are shown in Fig. 7A. The cephalocaudal distances for G. sup (points 3 and 4) were 22.05 ± 1.38 mm and 23.53 ± 1.61 mm, respectively, with the distance for G. sup significantly longer on the cleft side than on the non-cleft side ($p < 0.01$). The cephalocaudal distances for G. lat (points 5 and 6) were 28.47 ± 1.63 mm and 28.95 ± 1.66 mm, respectively. Those for G. base (points 8 and 9) were 34.74 ± 1.72 mm and 35.08 ± 1.80 mm, respectively, and those of Lt (points 11 and 12) were 47.56 ± 2.23 mm and 47.40 ± 2.26 mm, respectively. Comparisons of distances from the *x*-axis showed that those to points 5 and 6, to points 8 and 9, and to points 11 and 12 were not significantly different, indicating that the lower half of the nasal alar groove and Cupid's bow were restored to an almost symmetrical position (Fig. 7A).

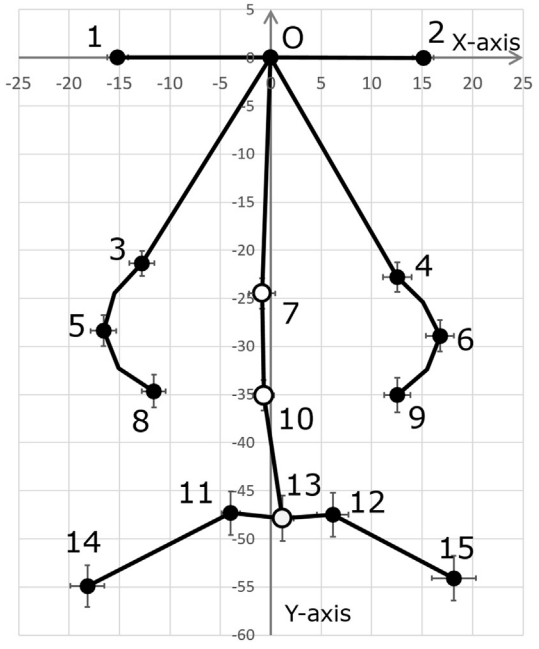

Fig. 6. The *x*- and *y*-coordinates of 17 facial landmarks were plotted in the *x*–*y* plane. The points Prm (point 7), Col (point 10), and Lm (point 12) are circled in white.

The anteroposterior distances from the *x*–*y* plane to the nasal alar and upper lip points are shown in Fig. 7B. The anteroposterior

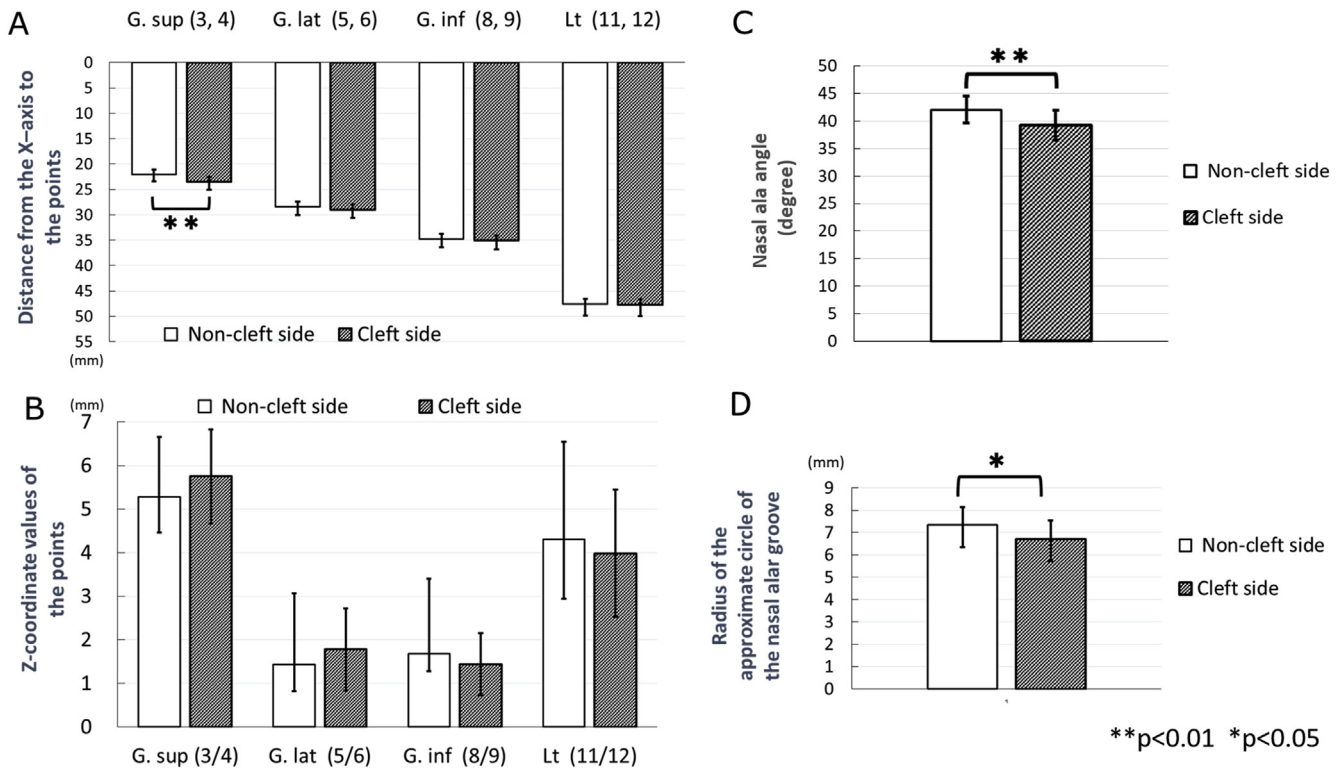

Fig. 7. (A) The distance from the *x*-axis to the points around the nasal alar and upper lip. The distance to G. sup on the cleft side was significantly longer than on the non-cleft side (**$p < 0.01$), but other points showed no significant differences between the cleft side and the non-cleft side. (B) The *z*-coordinates of the points around nasal alar and upper lip. These points showed no significant differences in anteroposterior position. (C) The nasal alar angle. The angle on the cleft side was significantly smaller than that on the non-cleft side (**$p < 0.01$). (D) The radius of the approximate circle of nasal alar. The curvature on the cleft side was significantly smaller than the non-cleft side (*$p < 0.05$).

distances for G. sup (points 3 and 4) were 5.28 ± 0.83 mm and 5.75 ± 1.08 mm, respectively; those for G. lat (points 5 and 6) were 1.43 ± 0.61 mm and 1.78 ± 0.94 mm, respectively; those for G. base (points 8 and 9) were 1.68 ± 0.40 mm and 1.44 ± 0.72 mm, respectively; and those for Lt (points 11 and 12) were 4.31 ± 1.37 mm and 3.98 ± 1.46 mm, respectively. Comparisons of the anteroposterior positions of these points showed no significant differences between the non-cleft and cleft sides. However, the upper half of the nasal alar on the cleft side tended to locate slightly more anteriorly than that on the non-cleft side, while the lower half of the nasal alar and upper lip on the cleft side was located slightly more posteriorly than that on the non-cleft side (Fig. 7B).

3.3. Assessment of the symmetry of nasal alar forms

The nasal alar angle on the cleft side was 39.29 ± 2.71°, and was significantly smaller than that on the non-cleft side (42.07 ± 2.47°; $p < 0.01$) (Fig. 7C).

The radius of the approximate circle of the nasal alar groove on the non-cleft side (R) was 7.34 ± 0.80 mm and that on the cleft side (r) was 6.72 ± 0.82 mm. A significant difference was observed in the radius of the nasal alar groove between the non-cleft and cleft sides ($p < 0.05$) (Fig. 7D). The ratio of curvature (r/R) was 0.92 ± 0.10.

3.4. Symmetry of the upper lip surface using histogram intersection

The values for similarity varied between 0.63 and 0.93. The mean and SD value for the upper lip surface on the non-cleft and cleft sides, calculated using histogram intersection, was 0.82 ± 0.07. Fig. 8 shows the contoured, color-coded images of the upper lip surface of the representative subjects, with both the high and low values of similarity. Subjects with higher values had more symmetrical contour lines in the visualized surface images. Furthermore, those with lower values had more asymmetrical contour lines in the visualized surface image, and the surface form of the portion corresponding to the philtrum column of the cleft side appeared flatter than that of the non-cleft side.

4. Discussion

The 3D scanning system based on stereophotogrammetry used in this study has a short image capturing time and is suitable for taking images of infants and young children (Al-Omari et al., 2005; He et al., 2010; Nakamura et al., 2010; Tse et al., 2014; Liang et al., 2017). Vectra H1® is compact and easily handled, and is able to rapidly capture facial images in clinical settings without the need for sedation.

According to the manufacturer, the geometry resolution (triangle edge length) of Vectra H1® is 0.80 mm. In an assessment of Vectra H1® using the 3dMD facial system, which has been widely used for analysing 3D images, the Vectra H1® system was found to be reliable for clinical applications (Camison et al., 2018). Nkenke et al. (2006) found that small measurement errors help to collect clinically relevant information. Previous studies have reported the reproducibility of the measuring points to be within 0.0–0.5 mm in evaluating morphological features of cleft-related deformity using 3D facial images (Hood et al., 2003; Bell et al., 2014). In this study, we analyzed the accuracy of the three points constituting the reference plane and the findings revealed that reliability was within 0.2 mm for the *x*-, *y*-, and *z*-coordinates. In addition, the reliability values for the 3D coordinates for each facial landmark were within 0.5 mm, except those for Ch for the *x*- and *z*-

Case	5Y3M M	4Y2M F	4Y3M M	5Y2M F
Value of similarity	0.93	0.92	0.65	0.63

Fig. 8. Values of similarity and the visualized contour lines on the upper lip surface images of four cases. The age (in years and months) and gender of the four cases are shown in the second row.

coordinates, which were greater than 0.8 mm. Regarding the low reliability of Ch, Hood et al. (2004) found that anthropometric measurements relating to lower lip and vertical mouth dimensions should not rely on the landmarks around the lip, because it is difficult for young children with clefts to perform 'lips together at rest'. Some reliability values were greater than 0.8 mm, while 75% of the measured values for all coordinates for each facial landmark were within 0.5 mm. Therefore the reference plane and facial landmarks of the 3D images in this study were considered to be reliable.

Although the results of these 3D analyses need to be interpreted with caution because of the relatively small sample size, several conclusions appear to be warranted. The first conclusion is that the postoperative nasolabial forms of our primary lip repair cases of children with complete UCLP had the following characteristics:

1) Regarding the medial line of the face, Prn and Col slightly dislocated to the non-cleft side, while the Lm of the upper lip shifted to the cleft side.
2) Regarding cephalocaudal heights on the cleft and non-cleft sides, G. lat, G. base, and Lt were restored to their symmetrical heights, while G. sup on the cleft side was still lower than that on the non-cleft side.
3) Asymmetry of the nasal alar angle and the radius of the curvature of the nasal alar groove between the cleft and non-cleft side remained.

Nasolabial morphology after lip repair using triangular repair for unilateral clefts often results in postoperative drooping of the nasal alar base and a long lip due to excessive elongation (Cronin, 1966; Brauer and Cronin, 1983). Although the design of the lip length on the affected side is recommended to be shorter (Cronin, 1966; Brauer and Cronin, 1983; Fisher, 2005), excessive extension of the upper lip has represented a major limitation of unilateral lip repair (Matsunaga et al., 2016). We previously reported that the simultaneous upward advancement of nasolabial components and anatomical reconstruction of the orbicularis muscle prevented postoperative nasolabial drooping and long lip according to 2D analysis (Nakamura et al., 2011; Matsunaga et al., 2016).

In this 3D analysis, we found that preoperative nasolabial tissue that had dislocated in the caudal direction was successfully re-established at the symmetrical height, and no excessive extension of the upper lip was observed. On the other hand, Prn, Col, and Lm were not recovered perfectly to the center of the face. Prm and Col had shifted slightly to the non-cleft side. Moreover, the position of Lm had shifted to the affected side.

In our department, we applied a NAM plate to correct the wide cleft space preoperatively. With this presurgical orthopedic treatment, the dislocated maxillary segments moved to the medial side, resulting in a narrow cleft space (Fuchigami et al., 2014), however, insufficient correction of the displaced upper maxillary segments may have retained the dislocation of Prn and Col from the center of the face in this study. Following the NAM treatment, the incisal point on the alveolar ridge of patients with UCLP was found to have moved excessively to almost the center of the face (Fuchigami et al., 2014). Furthermore, the collapse of maxillary segments may affect the shift in the position of Lm, because the soft tissue of the upper lip is pulled to the affected side as a result of muscle union during lip repair.

Okawachi et al. (2011) examined the angle of the nasal alar and the radius of the curvature of the nasal alar groove pre- and postoperatively, and reported that these were useful for assessing the symmetry of the nasal alar forms. In our study, we also adopted this approach for patients after primary lip repair, to assess the symmetry of the nose form. The results obtained showed that the asymmetry of the nasal form persisted. In our strategy for primary nose repair, NAM was applied for 3–4 months to recover the dome shape of the nose, and nasolabial tissue was simultaneously advanced upwardly to overlap the outer crus of the lower lateral cartilage on the upper lateral cartilage during lip repair. For nose correction, the nasal vestibule was then expanded with a cleft margin flap in the primary cleft lip surgery (Nakamura et al., 2011; Fuchigami et al., 2014; Matsunaga et al., 2016).

Our study revealed that G. sup on the cleft side was located more anteriorly and caudally than that on the non-cleft side. This issue may be attributed to many factors, such as anterior–posterior asymmetry of the maxillary bone, left and right differences in inherent nasal tissue volume, and insufficient upward advancement of the nasolabial tissue, including lower lateral cartilage, during lip repair. Therefore, we need to develop more successful presurgical orthopedics that will contribute to the recovery of maxillary bone around the nose and lip to the center of the face. We also need to employ countermeasures to improve the location of nasal cartilage to a more anatomically correct position in the future.

The histogram intersection method was shown to be useful because the upper lip surface form in patients with cleft lip and palate could be exhibited visually and quantified. Besides the white lip and vermilion, the upper lip has structural features called subunits, such as the philtrum ridge, philtrum dimple, and white roll. These are reconstructed through appropriate incision design and reconstruction of the orbicularis muscle during primary lip repair. Several surgeons have previously described surgical methods involving an incision line on the upper lip, approximating the subunit of the philtrum ridge (Cronin, 1966; Millard, 1976). The philtrum ridge and philtrum dimple are a result of the skin properties, as well as the alignment and thickness of the orbicularis oris muscle. Kim et al. (2017) reported that overlapping suturing on the orbicularis oris muscle can reproduce the natural, balanced appearance by creating an elevated philtrum ridge on the cleft side. Muscle repair needs to be accurate and precise in order to achieve successful results in lip repair surgery (Kuna et al., 2016). Lip repair in our study focused on anatomical reconstruction of the upper lip muscle, and the pars peripheralis of the orbicularis muscle was overlapped to produce the philtrum ridge in the upper lip (Nakamura et al., 2011; Matsunaga et al., 2016).

Accurate and global measurements of the skin surface can be difficult. Various methods have been previously employed to assess symmetry of the upper lip surface, both objectively and quantitatively. These have included superimposition of a 3D mirror image onto the original image (Desmedt et al., 2015; Mosmuller et al., 2017), the superimposition of pre- and postoperative 3D images with different colors (Okawachi et al., 2011; Al-Rudainy et al., 2018), and the comparison of face average UCLP models and healthy subjects to show differences in height by color and distance (distance map) (van Loon et al., 2010; Dadáková et al., 2016). However, there are difficulties associated with detecting the standard line for mirroring on the face in patients with complete UCLP. Therefore, symmetry of the upper lip skin surface in our study was evaluated using histogram intersection. Using this method, the degree of symmetry between the cleft side and non-cleft side could be evaluated without the need for a mirroring image. The similarity of the images was examined visually and compared with the numerically expressed value.

The results showed that symmetry of the upper lip surface of patients who underwent lip repair in our department varied from 0.8 to 0.9 to a value of 0.6. In this series, subjects with higher values had more symmetrical contour lines in the visualized surface images. On the other hand, those with lower values had more asymmetrical contour lines, and the surface form of the portion corresponding to the philtrum column of the cleft side appeared to be flattened. From these results, the histogram intersection method can be considered applicable as a method for quantitatively evaluating symmetry of the lip surface.

The relatively small samples in this study might be to be interpreted as a limitation. Moreover, a reference value of similarity in the upper lip surface form using the histogram intersection method has not yet been established. Future studies that compare the symmetry of the upper lip surface of cleft subjects with that of non-cleft subjects are needed in order to obtain a reference value for similarity.

5. Conclusions

The results of this study showed that the nasal alar base and Cupid's bow on the cleft side were restored to a symmetrical height, whereas a small nasal alar persisted postoperatively. The results also suggest that histogram intersection might be applicable as a method for quantitatively and objectively evaluating symmetry of the upper lip surface.

Ethical approval

This study was approved by the Kagoshima University Medical and Dental Hospital Institutional Review Board (# 28-192).

Declarations of interest

We declare that we have no conflict of interest.

Financial sources

There was no financial support for this work.

Patient consent

All participants provided informed consent.

Acknowledgements

None.

References

Al-Omari I, Millett DT, Ayoub AF: Methods of assessment of cleft-related facial deformity: a review. Cleft Palate Craniofac J 42(2): 145–156, 2005
Al-Rudainy D, Ju X, Mehendale F, Ayoub A: Assessment of facial asymmetry before and after the surgical repair of cleft lip in unilateral cleft lip and palate cases. Int J Oral Maxillofac Surg 47(3): 411–419, 2018
Bell A, Lo TW, Brown D, Bowman AW, Siebert JP, Simmons DR, et al: Three-dimensional assessment of facial appearance following surgical repair of unilateral cleft lip and palate. Cleft Palate Craniofac J 51(4): 462–471, 2014
Berssenbrügge P, Berlin NF, Kebeck G, Runte C, Jung S, Kleinheinz J, et al: 2D and 3D analysis methods of facial asymmetry in comparison. J Craniomaxillofac Surg 42(6): 327–334, 2014
Bilwatsch S, Kramer M, Haeusler G, Schuster M, Wurm J, Vairaktaris E, et al: Nasolabial symmetry following Tennison-Randall lip repair: a three-dimensional approach in 10-year-old patients with unilateral clefts of lip, alveolus and palate. J Craniomaxillofac Surg 34(5): 253–262, 2006
Brauer RO, Cronin TD: The Tennison lip repair revisited. Plast Reconstr Surg 71(5): 633–642, 1983
Bugaighis I, O'Higgins P, Tiddeman B, Mattick C, Ben Ali O, Hobson R: Three-dimensional geometric morphometrics applied to the study of children with cleft lip and/or palate from the North East of England. Eur J Orthod 32(5): 514–521, 2010
Camison L, Bykowski M, Lee WW, Carlson JC, Roosenboom J, Goldstein JA, et al: Validation of the Vectra H1 portable three-dimensional photogrammetry system for facial imaging. Int J Oral Maxillofac Surg 47(3): 403–410, 2018
Campbell A, Costello BJ, Ruiz RL: Cleft lip and palate surgery: an update of clinical outcomes for primary repair. Oral Maxillofac Surg Clin North Am 22(1): 43–58, 2010
Chou PY, Luo CC, Chen PK, Chen YR, Samuel Noordhoff M, Lo LJ: Preoperative lip measurement in patients with complete unilateral cleft/palate and its comparison with norms. J Plast Reconstr Aesthet Surg 66(4): 513–517, 2013
Cronin TD: A modification of the Tennison-type lip repair. Cleft Palate J 3: 376–382, 1966
Da Silveira AC, Daw Jr JL, Kusnoto B, Evans C, Cohen M: Craniofacial applications of three-dimensional laser surface scanning. J Craniofac Surg 14(4): 449–456, 2003
Dadáková M, Cagáňová V, Dupej J, Hoffmannová E, Borský J, Velemínská J: Three-dimensional evaluation of facial morphology in pre-school cleft patients following neonatal cheiloplasty. J Craniomaxillofac Surg 44(9): 1109–1116, 2016
Desmedt DJ, Maal TJ, Kuijpers MA, Bronkhorst EM, Kuijpers-Jagtman AM, Fudalej PS: Nasolabial symmetry and esthetics in cleft and palate: analysis of 3D facial images. Clin Oral Investig 19(8): 1833–1842, 2015
Fisher DM: Unilateral cleft lip repair: an anatomical subunit approximation technique. Plast Reconstr Surg 116(1): 61–71, 2005
Fuchigami T, Nakamura N, Nishihara K, Matsunaga K, Hasegawa H: Short-term molding effects on the upper alveolar arch following unilateral cleft lip repair with/without nasal vestibular expansion. Cleft Palate Craniofac J 51(5): 557–568, 2014
He X, Shi B, Jiang S, Li S, Zheng Q, Yan W: 110 infants with unrepaired unilateral cleft lip: an anthropometric analysis of the lip and nasal deformities. Int J Oral Maxillofac Surg 39(9): 847–852, 2010
Hood CA, Bock M, Hosey MT, Bowman A, Ayoub AF: Facial asymmetry — 3D assessment of infants with cleft lip & palate. Int J Paediatr Dent 13(6): 404–410, 2003
Hood CA, Hosey MT, Bock M, White J, Ray A, Ayoub AF: Facial characterization of infants with cleft lip and palate using a three-dimensional capture technique. Cleft Palate Craniofac J 41(1): 27–35, 2004
Kim HY, Park J, Chang MC, Song IS, Seo BM: Modified Fisher method for unilateral cleft lip — report of cases. Maxillofac Plast Reconstr Surg 5 39(1): 12, 2017
Knoops PG, Beaumont CA, Borghi A, Rodriguez-Florez N, Breakey RW, Rodgers W, et al: Comparison of three-dimensional scanner systems for craniomaxillofacial imaging. J Plast Reconstr Aesthet Surg 70(4): 441–449, 2017
Kuna SK, Srinath N, Naveen BS, Hasan K: Comparison of outcome of modified Millard's incision and Delaire's functional method in primary repair of unilateral cleft lip: a prospective study. J Maxillofac Oral Surg 15(2): 221–228, 2016
Li G, Wei J, Wang X, Wu G, Ma D, Wang B, et al: Three-dimensional facial anthropometry of unilateral cleft lip infants with a structured light scanning system. J Plast Reconstr Aesthet Surg 66(8): 1109–1116, 2013
Liang S, Shapiro L, Tse R: Measuring symmetry in children with cleft lip. Part 3: quantifying nasal symmetry and nasal normalcy before and after unilateral cleft lip repair. Cleft Palate Craniofac J 54(5): 602–611, 2017
Matsunaga K, Sasaguri M, Mitsuyasu T, Ohishi M, Nakamura N: Upward advancement of the nasolabial components at unilateral cleft lip repair prevents postoperative long lip. Cleft Palate Craniofac J 53(3): 71–80, 2016
Meyer-Marcotty P, Alpers GW, Gerdes AB, Stellzig-Eisenhauer A: Impact of facial asymmetry in visual perception: a 3-dimensional data analysis. Am J Orthod Dentofacial Orthop 137: 168.e1–168.e8, 2010
Millard DR: Cleft craft. In: The unilateral deformity, vol. 1. Boston: Little Brown, 581, 1976
Mosmuller D, Tan R, Mulder F, Bachour Y, de Vet H, Don Griot P: The use and reliability of SymNose for quantitative measurement of the nose and lip in unilateral cleft and palate patients. J Craniomaxillofac Surg 10: 1515–1521, 2016
Mosmuller DGM, Maal TJ, Prahl C, Tan RA, Mulder FJ, Schwirtz RMF, et al: Comparison of two- and three-dimensional assessment methods of nasolabial appearance in cleft lip and palate patients: do the assessment methods measure the same outcome? J Craniomaxillofac Surg 45(8): 1220–1226, 2017

Nakamura N, Sasaguri M, Nozoe E, Nishihara K, Hasegawa H, Nakamura S: Postoperative nasal forms after presurgical nasoalveolar molding followed by medial-upward advancement of nasolabial components with vestibular expansion for children with unilateral complete cleft lip and palate. J Oral Maxillofac Surg 67(10): 2222–2231, 2009

Nakamura N, Okawachi T, Nishihara K, Hirahara N, Nozoe E: Surgical technique for secondary correction of unilateral cleft lip-nose deformity: clinical and 3-dimensional observations of preoperative and postoperative nasal forms. J Oral Maxillofac Surg 68(9): 2248–2257, 2010

Nakamura N, Okawachi T, Nozoe E, Nishihara K, Matsunaga K: Three-dimensional analyses of nasal forms after secondary treatment of bilateral cleft lip-nose deformity in comparison to those of healthy young adults. J Oral Maxillofac Surg 69(11): e469–e481, 2011

Nkenke E, Lehner B, Kramer M, Haeusler G, Benz S, Schuster M, et al: Determination of facial symmetry in unilateral cleft lip and palate patients from three-dimensional data: technical report and assessment of measurement errors. Cleft Palate Craniofac J 43(2): 129–137, 2006

Okawachi T, Nozoe E, Nishihara K, Nakamura N: 3-dimensional analyses of outcomes following secondary treatment of unilateral cleft lip nose deformity. J Oral Maxillofac Surg 69(2): 322–332, 2011

Stauber I, Vairaktaris E, Holst A, Schuster M, Hirschfelder U, Neukam FW, et al: Three-dimensional analysis of facial symmetry in cleft lip and palate patients using optical surface data. J Orofac Orthop 69(4): 268–282, 2008

Swain MJ, Ballard DH: Color indexing. Int J Comput Vis 7(1): 11–32, 1991

Tse R, Booth L, Keys K, Saltzman B, Stuhaug E, Kapadia H, et al: Reliability of nasolabial anthropometric measures using three-dimensional stereophotogrammetry in infants with unrepaired unilateral cleft lip. Plast Reconstr Surg 133(4): 530e–542e, 2014

van Loon B, Maal TJ, Plooij JM, Ingels KJ, Borstlap WA, Kuijpers-Jagtman AM, et al: 3D stereophotogrammetric assessment of pre- and postoperative volumetric changes in the cleft lip and palate nose. Int J Oral Maxillofac Surg 39(6): 534–540, 2010

Wu J, Heike C, Birgfeld C, Evans K, Maga M, Morrison C, et al: Measuring symmetry in children with unrepaired cleft lip: defining a standard for the three-dimensional mid-facial reference plane. Cleft Palate Craniofac J 53(6): 695–704, 2016

Yamada T, Mori Y, Minami K, Mishima K, Sugahara T: Three-dimensional facial morphology, following primary cleft lip repair using triangular flap with or without rotation advancement. J Craniomaxillofac Surg 30(6): 337–342, 2002